Impact properties of novel corrosion resistant hybrid structures

E. Sarlin*, M. Apostol, M. Lindroos, V.-T. Kuokkala, J. Vuorinen, T. Lepistö, M. Vippola

Department of Materials Science, Tampere University of Technology, P.O. Box 589, 33101, Tampere, Finland

*Corresponding author: Essi Sarlin Tel. +358 408490146, E-mail: essi.sarlin@tut.fi

Abstract

The objectives of this study were to investigate the effect of impact energy and rubber thickness on the impact properties of layered steel/rubber/composite hybrid structures. Both stainless steel and mild steel based hybrid structures were investigated. The degree of damage, the failure modes, and the absorbed energy were studied.

It was found that rubber between steel and composite layers absorbs the impact energy and decreases the interfacial and internal damage in the studied hybrid structure and in its components. The amount of the absorbed energy did not change substantially when comparing structures with and without rubber. However, the area of permanent damage showed a decrease of nearly 50 % with the use of rubber when comparing a structure without rubber to a structure with 1.5 mm rubber. In addition, it was observed that the area of the damage is linearly dependent on the impact energy. The main damage mechanisms found were delamination at the steel/rubber and composite/rubber interfaces and fibre/matrix debonding in the composite layer.

Keywords: hybrid structure, high velocity impact, impact resistance.

1. Introduction

The current demand for energy savings and competitive industrial components requires new material solutions. Hybrid structures enable the combination of the best material properties of different material groups in one structure and thus offer interesting possibilities for new applications. In addition to high specific strength and stiffness, hybrids have a potential for other advantages, such as more beneficial manufacturing methods [1] or improved damping properties [2].

In our previous studies we have investigated the potential of steel/rubber/composite hybrid structures [3-6]. In these studies, the aim was to study the possibilities to attach glass fibre reinforced epoxy composite to stainless steel with the aid of a thin rubber layer. The research questions of our previous papers concentrated on the adhesion properties in laboratory conditions and in harsh environments as well as on the vibration damping properties. Since the adhesion of these structures was observed to be at a good level [3-4] and the rubber improves the energy absorption properties of the structure [6], we anticipated that our steel/rubber/composite structure has potential to be used also in real-life applications. However, the earlier studies did not show how the structure acts under transverse loading.

Composite structures are prone to damage induced by impacts in out-of-plane directions [7, 8]. The typical impact failure mechanisms of composite structures are matrix cracking and fibre fracture, fibre-matrix debonding and delamination, surface microbuckling and fibre shear out [9]. Similar to composites, laminated hybrid structures may exhibit both intra-layer and inter-layer damage under out-of-plane impacts [10]. One of the most established and studied polymer/metal hybrid structures are the Fibre Metal Laminates (FMLs). FMLs are shown to be less susceptible to impact loading than composites [11] leading to smaller damages [12]. Beyond FMLs, impact resistance of polymer/metal hybrid structures is not very widely studied. Some of the investigated structures are those combining brittle thermoplastics to aluminium or steel [e.g. 10, 13, 14]. Typical impact damage mechanisms found for polymer/metal hybrids are denting due to the plastic deformation of metal layers, epoxy and fibre cracking in the composite layers, and delamination [10, 14-17]. All in all, the knowledge of the damage mechanisms of hybrid structures under impact loading is essential for the prediction and simulation of the hybrid's behaviour in structural applications.

The impact test set-ups and test parameters used in literature vary widely. Typically, the impact tests are categorized according to the projectile velocity in low velocity (< 11 m/s), high velocity (> 11 m/s), and ballistic (> 500 m/s) impact tests [15]. Within composite structures, the low velocity damages emerge typically during maintenance and they may be visible only on the back side of the component, whereas the high velocity damages are more likely to emerge during the actual use of the application and they are typically visible on the impacted side [15, 18]. This paper concentrates on the high velocity impact loading.

In addition to standardized test geometries (e.g. ASTM D7136 or ASTM D6264), several more specific, in-house built test set-ups can be found in the literature. Minak and Ghelli [19] have studied the influence of specimen size and boundary conditions on the low velocity impact response of carbon fibre reinforced composites. Their rather intuitive result was that the impact behaviour of composites is dependent on both the specimen diameter and the boundary conditions through their effect on the specimen stiffness [19]. However, they also found that absorbed energy is independent on the boundary conditions and in-plane dimensions [19]. This result encourages using the absorbed energy as a test variable since it will not have any complex scaling effect.

In this study, the impact resistance of three different steel/rubber/composite hybrid structures was investigated. Two different Ethylene Propylene Diene (EPDM) based rubber grades for stainless steel based hybrids and one EPDM grade for mild steel based hybrids were used. The samples were exposed to high velocity impact loading. The failure modes and the energy absorption of the samples were compared to the impact energy and to the rubber thickness of the samples. The failure modes were studied from the cross-sectional samples with scanning electron microscopy, while the energy absorption of the samples was evaluated with the aid of a high speed video system.

2. Experimental

2.1 Materials

In this study, the impact properties of steel/rubber/composite hybrid structures were investigated. Three different specimen types were used: two based on stainless steel and one based on mild steel. The steel grades used were stainless steel AISI 304 (provided by Outokumpu Stainless Oy, Finland) and passivation treated cold rolled mild steel EN 10130 DC01 (provided by Rautaruukki Oyj, Finland). The thickness of the steel sheets was 0.5 mm. The surface finish of the stainless steel was industrial 2D (cold rolled, heat treated, pickled), while the mild steel surface was cold rolled and passivation treated. Prior to rubber bonding, the steel sheets were rinsed with acetone and ethanol. Other pre-treatments, such as grit blasting, were not used.

The glass fibre reinforced epoxy composite sheets were manufactured in-house by vacuum infusion from stitched 0/90 E-glass fibre fabrics (682 g/m^2, from Ahlstrom Oyj, Finland) and Sicomin SR 1660 / SD 7820 epoxy (from Sicomin Composites, UK). The nominal thickness of the composite sheets was 3.5 mm consisting of 6 layers of fabrics. The fibre content of the composite was about 46 vol-%. The heat resistant epoxy was chosen to provide the good resistance of the GFRP sheet to the vulcanizing temperature used for the rubbers. From the adhered composite surface, a HexForce® T470 (Hexcel Co., USA) peel ply was removed prior to rubber attachment. The peel ply creates a rough composite surface.

Three different Ethylene Propylene Diene (EPDM) based rubber grades, grade A manufactured by Teknikum Oy, Finland and grades B and C manufactured by Kraiburg GmbH, Germany, were used to adhere the steel and the composite sheets together. The hybrid structures were manufactured by vulcanizing the rubber between the metal and the composite layers under heat and pressure (at 1.2 MPa and 130-160°C depending on the rubber grade). Three nominal rubber thicknesses, 0.5 mm, 1.0 mm and 1.5 mm, were used. Thin metal plates between the steel and the composite sheets ensured uniform rubber thicknesses during the vulcanization. In addition, as a reference a commercial epoxy adhesive 3M™ Scotch-Weld™ Epoxy Adhesive DP190 Gray was used to produce steel/composite samples with no rubber between (i.e., zero rubber thickness). This adhesive exhibits good peel, shear and environmental aging properties. The studied samples and the test parameters are summarized in Table 1. Three samples were tested with each test parameter combination.

2.2 Methods

The impact test equipment was an in-house developed High Velocity Particle Impactor (HVPI). In this device, compressed air is used to fire a 9 mm diameter projectile towards the sample. The velocity of the projectile is determined by a computer controlled pressure reservoir and the projectile velocity is recorded with a commercial ballistic chronograph placed in front of the target assembly. The test setup allows a wide range of impact angles to be studied approximately from 10° to 90°. The impact event is recorded with a high speed camera (NAC Memrecam fx K5, NAC Image Technology, USA). The high speed video

images were recorded at a constant frame rate of 40000 fps. The HVPI equipment is fully computer controlled.

In this study, through hardened steel balls (2.98 g in weight) were used as projectiles. The specimen angle was set to 45°±1° as a compromise between the two extremes. The pressure was varied between 1-14 bar, leading to the velocities for the steel balls between 44-142 m/s and the corresponding energies of 3-30 J. The 50×50 mm size samples were fixed with the steel side upwards in a 130×130 mm aluminium clamp. The clamp had a circular opening of 40 mm in the centre. The geometry enables the sample to bend during the impact. When determining the size of the clamp opening, it was designed to exceed the size of the maximum damage at 30 J but simultaneously to minimize the sample material consumption. The round clamp opening was chosen to create a spherical boundary condition. Schematic presentations of the test set-up, the clamp and the sample geometry are shown in Figs. 1 and 2.

The dissipated energy E_d of the projectile was calculated by comparing the initial and post-impact kinetic energy of the projectile according to Equation 1:

$$E_d = \frac{1}{2} m_p \left(v_i - \frac{\Delta s}{\Delta t} \right)^2 \quad (1)$$

where m_p, v_i, Δs, Δt are the projectile's mass and initial velocity, displacement of a sample point between two images and the time consumed for this displacement of the projectile, respectively. The initial velocity was measured with the ballistic chronograph placed in front of the sample. A custom image analysis suite was used to estimate the velocity of the projectiles after the impact by overlaying two post-impact images from the high speed photographs, where the projectile is no more in contact with the specimen. Since the spherical shape of the projectile allows tracking of the same material point in the images, e.g. the centre of the sphere, the distance travelled by the projectile was calculated from the overlaid image and divided by the time consumed for this displacement. A small error is involved in the distance calculations due to a slightly angular position of the camera, but due to its negligible influence on the accuracy of the results, it was omitted. The mass change of the projectile during the impact was also assumed to be negligible since the projectile remains intact and has no sign of noticeable wear or increase in mass due to adhesion from the counter-surface.

After the impact tests, the samples were further studied visually by photographing them from the impacted steel surface and from the composite (back) side. In addition, cross sectional studies were done with Scanning Electron Microscope (SEM) Zeiss ULTRAplus. Conventional metallographic cross-sectional sample preparation method, including cutting the sample from the original specimens, mounting in epoxy, grinding, and polishing, was used to prepare the cross-sectional samples for SEM. Prior to SEM investigations the samples were coated with a thin gold coating to ensure their conductivity under the electron beam.

3. Results

Visual inspection of the samples revealed that the projectile impact caused plastic deformation in the steel surface and different types of damage in the composite sheet (Fig. 3). The shape of the impact crater was droplet-like due to the impact angle less than 90°, and at higher impact energies (15 and 30 J) the composite damage area exceeded the impact crater area in the steel sheet. In this study, the damage size of the composite layer is described by the maximum damage diameter (MDD) and by the damage area. The MDD and damage area values were determined from the photographs by using an image processing program, as shown in Fig. 3.c.

3.1 The effect of rubber thickness

The damage area versus the rubber thickness is shown in Fig. 4.a. The use of rubber instead of epoxy decreased the damage area by 26-47 % for the stainless steel based hybrids and by 4-23 % for the mild steel based hybrids, depending on the rubber thickness. However, for rubber types A and C the increase in the rubber thickness from 0.5 to 1.5 mm did not decrease the damage size markedly but it rather stayed within the standard deviation limits. Only rubber type B showed a decreasing trend with increasing rubber thickness. In addition to the small error involved in the distance calculations, origins for the scatter in the test results are, for example, local variations in the rubber and/or composite thickness and the small variations in the tension of the clamp screws.

The energy absorbed by the hybrid structures during the impact event versus the rubber thickness are shown in Fig. 4.b. In general, the amount of absorbed impact energy was 70-77 % of the original 15 joules. Contrary to the maximum damage diameters, the dissipated energy did not seem to depend on the existence or thickness of the rubber layer.

3.2 The effect of impact energy

A diagram of MDD and the damage area versus impact energy are shown in Fig. 5. At the studied energy range, the damage area showed linear behaviour and the deviation of the results was moderate. When comparing the amount of absorbed energy to the impact energy (Fig. 6), the dependence is seen not to be linear.

3.3 Characterization of the damage mechanisms

Cross-sectional SEM images of the impact craters of samples impacted with 3 J and 30 J are shown in Fig. 7. At high impact energies, the rebound of the projectile off from the surface caused a secondary crater, as seen also in Fig. 7.b. These “rebound craters” increased the size of the plastically deformed area in steel plates so that the higher rubber thickness led to larger crater dimensions in the case of mild steel samples (Table 2). The crater dimensions were measured from one of the three tested plates with intermediate MDD value for each sample type. For the stainless steel samples, the crater lengths showed slight decrease with increasing rubber thickness. No clear trend in the depths of the impact craters was observed with rubber thickness. However, increase in the impact energy showed clear increase in the crater length.

According to the SEM studies, the primary damage mechanisms of the steel/rubber/composite hybrids were interfacial delamination and fibre/matrix debonding (Fig. 8). In general, the most clearly delaminated parts were concentrated on the areas where the plastic deformation of steel was strongest, as shown schematically in Fig. 9. The central areas of the impact craters had typically a tight contact between the components. No steel/rubber delaminations were found and only a few delaminated stretches of interface were found between the composite and the rubber in the central areas of the impact craters.

Outside the impact crater, the delaminated areas did not appear to be continuous throughout the delamination width on either of the interfaces. However, when observing and analysing delamination by SEM, it should be kept in mind that grinding, as part of the sample preparation process, may cause changes in the delamination dimensions at the sample surface. Delamination can be expanded by peeling the components apart, or reduced by smearing the rubber over the other component. Thus, especially the steel/rubber delamination cannot be reliably determined by SEM studies. The visual inspection of the delamination at the composite/rubber interface is possible due to the transparency of the composite sheet, and the interfacial delamination was not observed to exceed the damaged area of the composite, which is opaque. In the samples without rubber, delamination at the steel/epoxy interface was found, whereas the composite/epoxy interfaces were intact. However, no clear difference in the composite damage density was found when compared to the rubber bonded samples.

Generally, non-destructive methods should be used to evaluate the extent of delaminations in impact loaded composite samples. The authors' plan was to apply a Scanning Acoustic Microscope (SAM) to find out the dimensions of the delamination at the steel/rubber interface. However, the multi-layered hybrid structure and the internal structure of the composite layer caused so complex return echoes that even the analysis of the initial samples was not possible.

The damage density in the composite layers was surprisingly low when compared to the visual appearance of the samples. The samples impacted with 30 J showed higher damage density than the other ones. In addition to fibre/matrix debonding, fibre breakage and matrix cracks (Fig. 10) were found to a minor extent. Due to the translucent nature of the intact composite, the dimensions of the damaged area in the composite are more reliably determined visually than by SEM. In addition, delamination at the composite/rubber interfaces would be visible under the intact composite, but the delaminated area at that interface did not exceed the area of the damaged composite. Internal damage in the stainless steel or in the rubber layers was not found, and only a few surface fractures at the mild steel/rubber interface were observed. However, since the used steel sheets were in as-received stage, it cannot be said if these fractures were already in the steel before hybrid manufacturing, if they were induced by the impact or if they were artefacts of the sample preparation process.

4. Discussion

The rubber thickness versus damage size studies showed that the rubber layer absorbs the impact energy and decreases the interfacial and internal damage in the hybrid structure and in its components. The 47% decrease in the damage area in the stainless steel based hybrid with 1.5 mm rubber B layer is a very promising result, especially when taking into account the previous results of the adhesion studies [3, 4], which showed that the use of a rubber layer removes the need for steel pre-treatments. Thus the studied structure is a promising choice for real life applications such as impact loaded stressed-skin constructions.

Even though the use of rubber does not change markedly the amount of absorbed energy, it obviously changes the energy absorption mechanisms: instead of causing permanent damage in the composite layer, rubber absorbs the energy. Generally the energy is lost in viscous systems (such as rubber) by heat build-up [21]. This change in the energy absorption mechanism can be seen in the decreased damage size.

The linear dependency between the damage area and the impact energy is expected and makes the evaluation of the hybrid structures' suitability for industrial applications easier. In addition, the results of the energy absorption versus the impact crater size are in line with this finding. When comparing the impact energy and absorbed energy in the Energy Profiling Diagram (EPD) in Fig. 11, it can be seen that the relative amount of absorbed energy decreases with increasing impact energy. However, if the impact energy would further increase, the EPD curve would turn towards the equal-energy line and finally encounter it through penetration and perforation. This kind of shape is typical for the EPD curve of composite structures [7, 22, 23].

The difference in the impact crater size of the mild and stainless steel based hybrids can be attributed to the higher strength of the mild steel (yield strength 300 MPa [24]) compared with the stainless steel (yield strength 230 MPa [25]). In addition, the Shore D hardness of the rubbers A, B and C are 41, 43 and 44 [4], respectively, which may have had an effect on the crater size as well. The higher crater depth in the samples with a thick rubber layer can be explained by the higher deformability of those samples. From the design point of view, no reason for high rubber thickness is evident especially in the case of rubbers A and B. In addition to the size of the damage areas, this conclusion is supported by the result of the authors' previous study [5], which showed increasing adhesion strength with decreasing rubber thickness. However, the decreasing trend in the damage area with increasing rubber B thickness implies that optimization between the impact and adhesion properties must be done when designing the final structure.

Since the density of fibre/matrix debonding was higher than the density of fibre breaks or matrix cracks, the fibre/matrix interface must be the weakest point of the composite. Still, the extent and the density of fibre/matrix debonding damages were surprisingly low in samples impacted with 3J or 15J, and thus the authors assume that the residual strength of the hybrid structures is not dramatically decreased. However, to ensure this assumption, compression after impact (CAI) tests (according to ASTM D7137), for example, could be done, since the

compressive strength is typically the limiting factor of composite materials in load bearing applications [26].

5. Conclusions

In this study, the impact resistance and fracture mechanisms of mild and stainless steel/rubber/composite hybrid structures under impact loading were studied. Samples with different rubber thicknesses were subjected to high velocity impacts at different energies. According to the results of this study, the following conclusion can be made:

- A thin rubber layer between the steel and the composite does not decrease the amount of absorbed energy markedly but changes the energy absorption mechanisms protecting the structure from permanent damage. In this study, a decrease of nearly 50 % in the damage area was achieved by a 1.5 mm rubber layer in the stainless steel/rubber/composite hybrid structure.
- The increase of rubber thickness within the studied range of 0.5 to 1.5 mm did not have a strong effect on the damage area. The most marked decrease in the damage area was observed between the structures without rubber and the structures with the thinnest rubber layer.
- The damage area is linearly dependent on the impact energy in the studied energy range (3-30 J). This could facilitate the evaluation of the expected damage under known impact load level of an industrial application.
- The main damage mechanisms of the hybrids under impact loading were delamination between the components and fibre/matrix debonding in the composite layer.

Due to the improved impact properties and the simple manufacturing process, the use of rubber as a thin adhesive layer between stainless steel and composite can be recommended to be implemented in real life applications such as impact loaded stressed-skin constructions.

Acknowledges

The work was funded by the Doctoral Programme of TUT's President (E. Sarlin), by FIMECC Ltd and its Demanding Applications program (M. Apostol, M. Lindroos and V.-T. Kuokkala) and Light and Efficient Solutions Program (J. Vuorinen). The authors acknowledge Outokumpu Stainless Oy for the stainless steel sheets, Rautaruukki Oyj for the cold rolled steel sheets, and Kraiburg GmbH and Teknikum Oy for the rubbers. We are grateful for Kosti Rämö, Niko Polet, Olli Partanen and Atte Antikainen from Tampere University of Technology (TUT) for preparing the samples used in this work.

References

[1]: LANXESS. Plastic metal hybrid technology. [WWW] [17.6.2013] Available in: http://techcenter.lanxess.com/scp/americas/en/innoscp/tech/78310/article.jsp?docId=78310

[2]: Ghiringhelli GL, Terraneo M, Vigoni E. Improvement of structures vibroacoustics by widespread embodiment of viscoelastic materials. Aerospace Science and Technology 2013;28(1):227–241.

[3]: Sarlin E, Heinonen E, Vuorinen J, Vippola M, Lepistö T. Adhesion properties of novel corrosion resistant hybrid structures. Submitted to International Journal of Adhesion and Adhesives.

[4]: Sarlin E, Hoikkanen M, Frisk L, Vuorinen J, Vippola M, Lepistö T. Ageing of corrosion resistant steel/rubber/composite hybrid structures. Submitted to International Journal of Adhesion and Adhesives.

[5]: Sarlin E, Vuorinen J, Vippola M, Lepistö T. The effect of rubber thickness and load rate on the interfacial fracture energy in steel/rubber/composite hybrid structures. In: Proceedings of 19th International Conference on Composite Materials, Montreal; 27 July – 2 August, 2013.

[6]: Sarlin E, Liu Y, Vippola M, Zogg M, Ermanni P, Vuorinen J, Lepistö T. Vibration damping properties of steel/rubber/composite hybrid structures. Composite Structures 2013;94(11):3327–3335.

[7]: Sayer M, Bektaş NM, Demir E, Çallioğlu H. The effect of temperatures on hybrid composite laminates under impact loading. Composites: Part B 2012;43(5):2152-2160.

[8]: Hosur MV, Jain K, Chowdhury F, Jeelani S, Bhat MR, Murthy CRL. Low-velocity impact response of carbon/epoxy laminates subjected to cold–dry and cold–moist conditioning. Composite Structures 2007;79(2):300-311.

[9]: Davies GAO, Hitchings D. Impact damage and residual strengths of woven fabric glass/polyester laminates. Composites: Part A 1996;27:1147-1156.

[10]. Xu LR, Rosakis AJ. Impact failure characteristics in sandwich structures Part I: Basic failure mode selection. International journal of solid and structures 2002;39:4215-4235.

[11]: Yang J-M, Hahn HT, Seo H. Impact damage tolerance and fatigue durability of GLARE laminates. Journal of Engineering Materials and Technology 2008;130.

[12]: Vlot A. Impact loading on fibre metal laminates. International Journal of Impact Engineering 1996;18(3):291-307.

[13]: Liu X, Liaw B. Drop-weight impact tests and finite element modeling of cast acrylic/aluminum plates. Polymer Testing 2009;28:808-823.

[14]: Lambros J, Rosakis AJ. Shear dominated transonic interfacial crack growth in a bimaterial – I. Experimental observation. Journal of the Mechanics and Physics of Solids 1995;43(2):169-188.

[15]: Hagenbeek M. Impact properties. In: Vlot A, Gunnink, JW, editors. Fibre metal laminates: An introduction. Dordrecht: Kluwer Academic Publishers, 2001, pp. 409-426.

[16]: Langdon GS, Rowe LA. The response of steel-based fibre-metal laminates to localised blast loading. In: Proceedings of 17th International Conference on Composite Materials, Edinburgh; 27-31 July, 2009.

[17]: Abdullah MR, Cantwell WJ. The impact resistance of polypropylene-based fibre-metal laminates. Composites Science and Technology 2006;66:1682-1693.

[18]: Hosseinzadeh R, Shokrieh MM, Lessard L. Damage behaviour of fiber reinforced composite plates subjected to drop weight impacts. Composites Science and Technology 2006;66:61-68.

[19]: Minak G, Ghelli D. Influence of diameter and boundary conditions on low velocity impact response of CFRP circular laminated plates. Composites Part B 2008;39(6):962-972.

[20]: Apostol M, Kuokkala VT, Laukkanen A, Holmberg K, Waudby R, Lindroos M. High velocity particle impactor – modelling and experimental verification of impact wear tests. In: Proceedings of the World Tribology Congress, Torino; 8-13 September, 2013.

[21]. Ungar EE. Damping of structures and use of damping materials. In: Crocker MJ (Editor). Handbook of Noise and Vibration Control. John Wiley & Sons, 2007, pp. 734-744.

[22]: Sayer M, Bektaş NM, Sayman O. An experimental investigation on the impact behaviour of hybrid composite plates. Composite Structures 2010;92:1256-1262.

[23]. Belingardi G, Cavatorta MP, Paolino DS. On the rate of growth and extent of the steady damage accumulation phase in repeated impacts. Composites Science and Technology 2009;69:1693-1698.

[24]: Ruukki. Formable steels EN 10130. [WWW] [5.6.2013] Available in: http://www.ruukki.com/formablesteels

[25]: Outokumpu. Standard Cr-Ni Stainless Steels. [WWW] [5.6.2013] Available in: http://www.outokumpu.com/SiteCollectionDocuments/Austenitic_Standard_Grades_Datasheet.pdf

[26]: Schultheisz CR, Waas AM. Compressive failure of composites, Part I: Testing and micromechanical theories. Progress in Aerospace Sciences 1996;32:1-42.

Tables and Figures

Table 1: Studied sample components with nominal thicknesses and applied impact energies.

<table>
<tr><td colspan="4">To study the effect of rubber thickness</td></tr>
<tr><td>Steel</td><td>Adhesive</td><td>Composite</td><td>Impact energy</td></tr>
<tr><td rowspan="8">Stainless steel
AISI 304 0.5 mm</td><td>Rubber A 0.5 mm</td><td rowspan="12">GFRP 3.5 mm</td><td rowspan="12">15 J</td></tr>
<tr><td>Rubber A 1.0 mm</td></tr>
<tr><td>Rubber A 1.5 mm</td></tr>
<tr><td>Rubber B 0.5 mm</td></tr>
<tr><td>Rubber B 1.0 mm</td></tr>
<tr><td>Rubber B 1.5 mm</td></tr>
<tr><td>Epoxy adhesive</td></tr>
<tr><td rowspan="4">Mild steel
EN10130 DC01 0.5 mm</td><td>Rubber C 0.5 mm</td></tr>
<tr><td>Rubber C 1.0 mm</td></tr>
<tr><td>Rubber C 1.5 mm</td></tr>
<tr><td>Epoxy adhesive</td></tr>
<tr><td colspan="4">To study the effect of impact energy</td></tr>
<tr><td>Steel</td><td>Adhesive</td><td>Composite</td><td>Impact energy</td></tr>
<tr><td rowspan="3">Stainless steel
AISI 304 0.5 mm</td><td rowspan="3">Rubber A 1.0 mm</td><td rowspan="3">GFRP 3.5 mm</td><td>3 J</td></tr>
<tr><td>15 J</td></tr>
<tr><td>30 J</td></tr>
</table>

Table 2: Length and depth of impact craters estimated from SEM images.

To study the effect of rubber thickness			
Steel	***Adhesive***	***Composite***	***Impact energy***
Stainless steel AISI 304 0.5 mm	*Rubber A 0.5 mm*	*GFRP 3.5 mm*	*15 J*
	Rubber A 1.0 mm		
	Rubber A 1.5 mm		
	Rubber B 0.5 mm		
	Rubber B 1.0 mm		
	Rubber B 1.5 mm		
	Epoxy adhesive		
Mild steel EN10130 DC01 0.5 mm	*Rubber C 0.5 mm*		
	Rubber C 1.0 mm		
	Rubber C 1.5 mm		
	Epoxy adhesive		
To study the effect of impact energy			
Steel	***Adhesive***	***Composite***	***Impact energy***
Stainless steel AISI 304 0.5 mm	*Rubber A 1.0 mm*	*GFRP 3.5 mm*	*3 J*
			15 J
			30 J

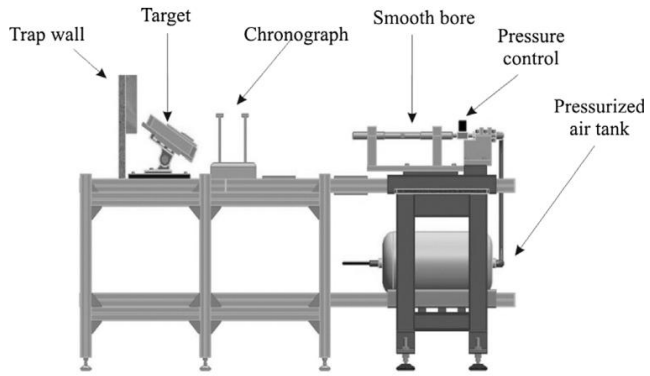

Fig. 1: A schematic presentation of the high velocity impact test set-up [20].

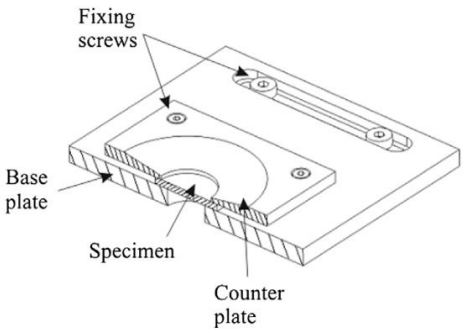

Fig. 2: A schematic section view of the sample holder.

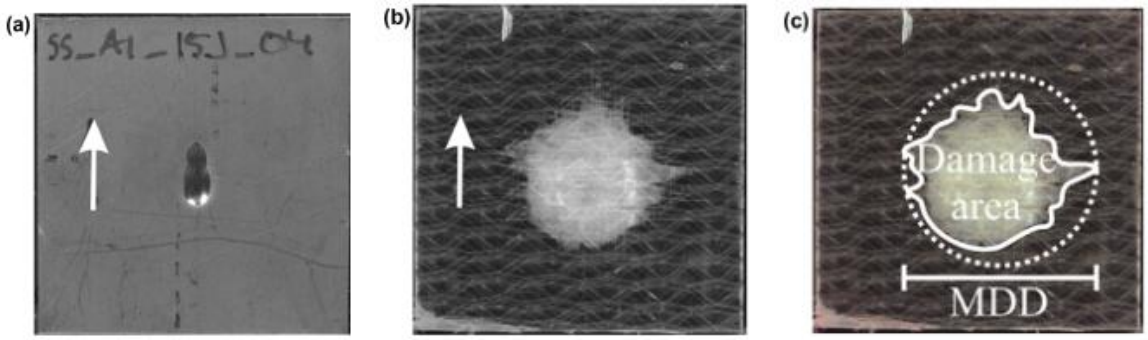

Fig. 3: Impact tested stainless steel/rubber A/composite hybrid sample a) from the steel and b) from the composite side. In c) the MDD and the damage area are shown. The arrows in Figs. a) and b) show the direction of the impact.

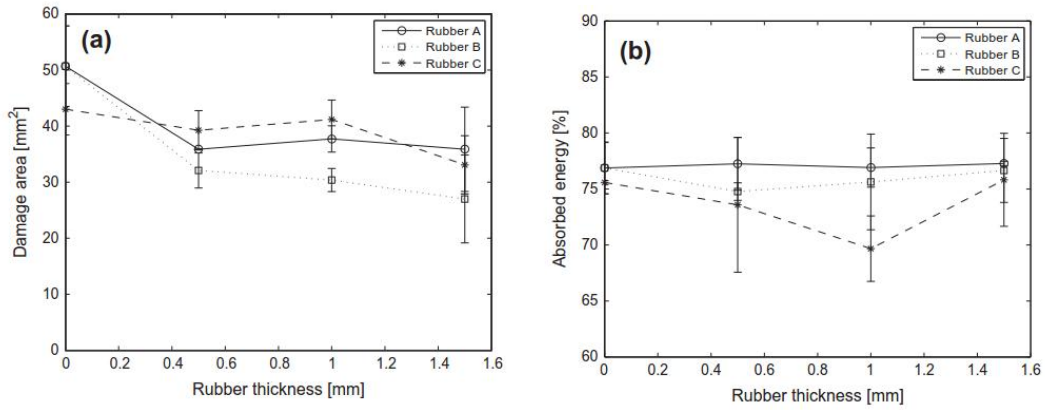

Fig. 4: a) effect of rubber thickness on the damage area and b) effect of rubber thickness on the dissipated energy in percentage for two stainless steel based samples (Rubbers A and B) and for a mild steel based sample (Rubber C).

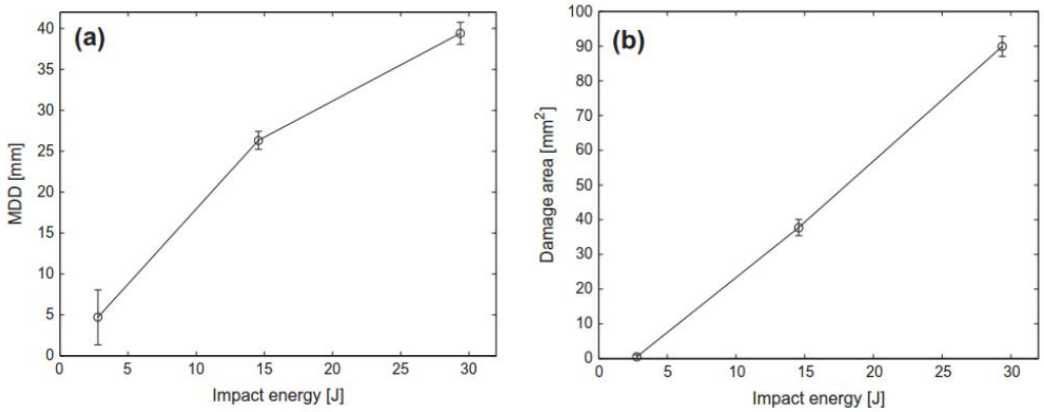

Fig. 5: a) MDD versus impact energy and b) damage area versus impact energy for the stainless steel/rubber/composite hybrid with a nominal rubber thickness of 1 mm.

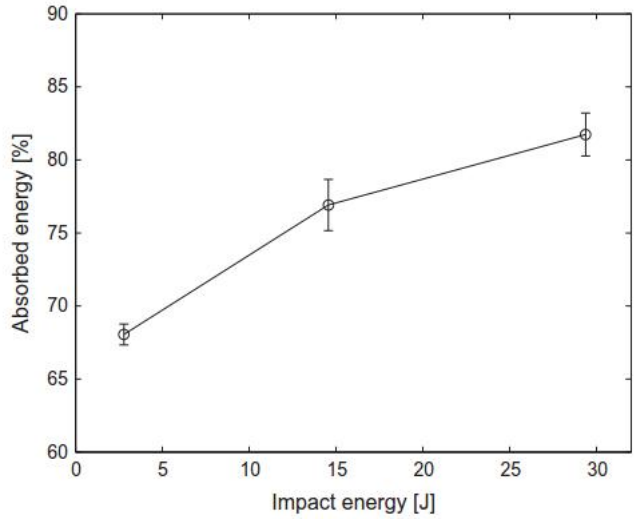

Fig. 6: Absorbed energy versus impact energy for the stainless steel/rubber/composite hybrid with a nominal rubber thickness of 1 mm.

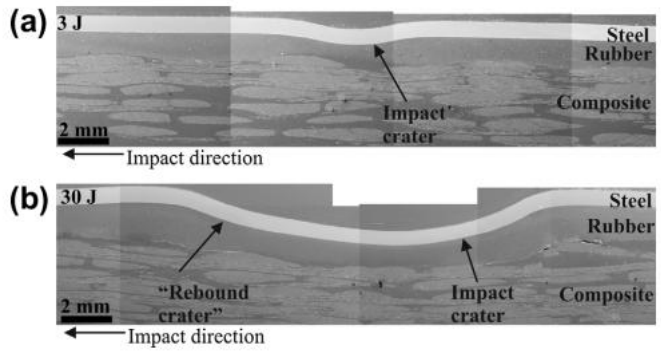

Fig. 7: Cross sectional SEM images from the stainless steel/rubber A/composite samples. The impact energies are a) 3J and b) 30 J.

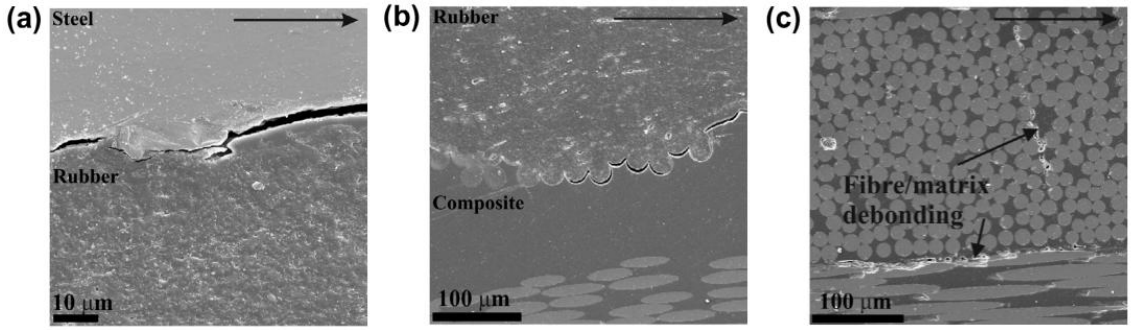

Fig. 8: The main damage mechanisms: a) steel/rubber delamination b) composite/rubber delamination and c) fibre/matrix debonding. The arrow shows the direction of the impact.

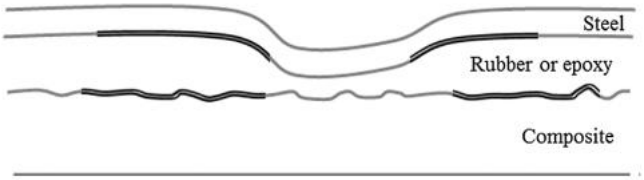

Fig. 9: Schematic presentation of the typical locations of delaminations.

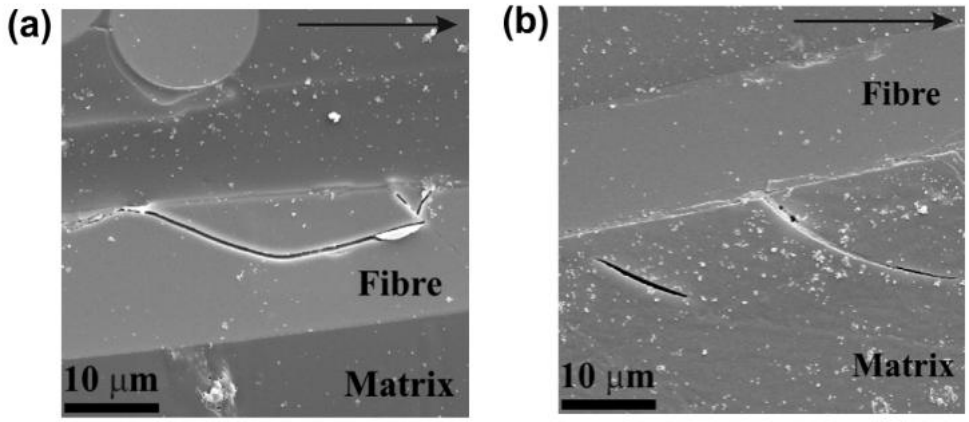

Fig. 10: Examples of other damage mechanisms: a) fibre breakage and b) matrix cracking. The arrow shows the direction of the impact.

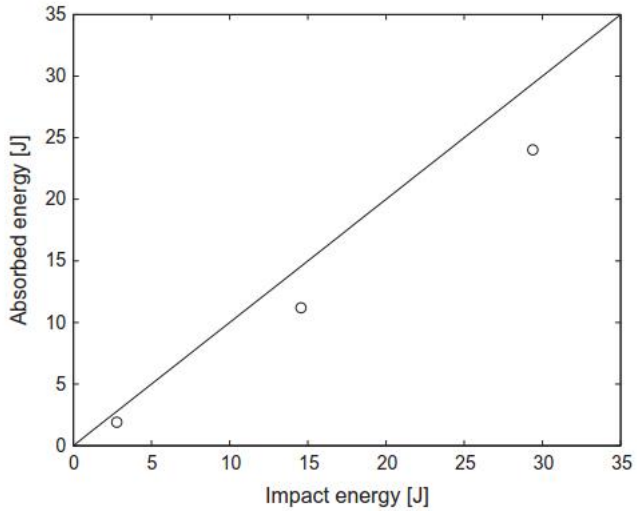

Fig. 11: Energy profile diagram of the stainless steel/rubber A/composite hybrid structure (rubber thickness 1.0 mm).